C&B DRUG DESIGN   WILEY

Antihypertensive activity and molecular interactions of irbesartan in complex with 2-hydroxypropyl-β-cyclodextrin

Georgios Leonis[1] | Eirini Christodoulou[1] (iD) | Dimitrios Ntountaniotis[1] |
Maria V. Chatziathanasiadou[2] | Thomas Mavromoustakos[1] (iD) | Nikolaos Naziris[3] (iD) |
Maria Chountoulesi[3] | Costas Demetzos[3] | Georgia Valsami[3] | Dimitrios E. Damalas[4] (iD) |
Andreas G. Tzakos[2] | Nikolaos S. Thomaidis[4] | Vlasios Karageorgos[5] | Georgios Liapakis[5]

[1]Laboratory of Organic Chemistry, Department of Chemistry, National and Kapodistrian University of Athens, Zografou, Greece

[2]Department of Chemistry, Section of Organic Chemistry and Biochemistry, University of Ioannina, Ioannina, Greece

[3]Section of Pharmaceutical Technology, Department of Pharmacy, School of Health Sciences, National and Kapodistrian University of Athens, Athens, Greece

[4]Department of Chemistry, Laboratory of Analytical Chemistry, National and Kapodistrian University of Athens, Zografou, Greece

[5]Department of Basic Sciences, School of Medicine, University of Crete, Heraklion, Crete, Greece

Correspondence
Georgios Leonis, Eirini Christodoulou, Dimitrios Ntountaniotis and Thomas Mavromoustakos, Laboratory of Organic Chemistry, Department of Chemistry, National and Kapodistrian University of Athens, Panepistimioupolis, Zografou 15771, Greece.
Emails: georgios.leonis@gmail.com; e_christod@pharm.uoa.gr; doudaniotis@yahoo.gr; tmavrom@chem.uoa.gr

Abstract

Irbesartan (IRB) exerts beneficial effects either alone or in combination with other drugs on numerous diseases, such as cancer, diabetes, and hypertension. However, due to its high lipophilicity, IRB does not possess the optimum pharmacological efficiency. To circumvent this problem, a drug delivery system with 2-hydroxypropyl-β-cyclodextrin (2-HP-β-CD) was explored. The 1:1 complex between IRB and 2-HP-β-CD was identified through ESI QTF HRMS. Dissolution studies showed a higher dissolution rate of the lyophilized IRB–2-HP-β-CD complex than the tablet containing IRB at pH = 1.2. DSC results revealed the differences of the thermal properties between the complex and various mixtures consisting of the two components, namely IRB and 2-HP-β-CD. Interestingly, depending on the way the mixture preparation was conducted, different association between the two components was observed. Molecular dynamics (MD) simulations predicted the favorable formation of the above complex and identified the dominant interactions between IRB and 2-HP-β-CD. *In vitro* pharmacological results verified that the inclusion complex not only preserves the binding affinity of IRB for AT1R receptor, but also it slightly increases it. As the complex formulation lacks the problems of the tablet, our approach is a promising new way to improve the efficiency of IRB.

KEYWORDS

2-hydroxypropyl-β-cyclodextrin, binding assays, differential scanning calorimetry, hypertension, irbesartan, mass spectrometry, molecular dynamics

1 | INTRODUCTION

Eight angiotensin II (AII) type 1 receptor (AT1R) blockers (ARBs) have been developed and marketed as drugs against hypertension. These pharmaceutical molecules are structural derivatives of the prototype drug losartan and constitute the class of sartans. Structurally, they are characterized by (a) an acidic biphenyltetrazole segment or a biphenyl or phenyl ring with an attached carboxylate group and (b) a single or condensed heterocyclic ring bearing a hydrophobic group. Their molecular mechanism of action is still unresolved and may involve either a direct action on AT1R or their insertion and diffusion through lipid bilayers before reaching the receptor (Tamargo et al., 2015; Kellici, Ntountaniotis, et al., 2016). After reaching AT1R, the molecules act as Trojan horses deceiving AII and preventing its binding from exerting its detrimental antihypertensive effect.

Although sartans act on the same target, it has been found that they have distinct pharmacological profiles, with irbesartan (IRB, trade name Aprovel, 2-butyl-3-[p-(o-1H tetrazol-5-ylphenyl) benzyl]-1,3-diazaspiro [4.4] non-1-en-4-one, Figure 1) being superior to others (Adams & Trudeau 2000; Kellici, Liapakis, et al., 2015). IRB is beneficial either alone or in combination with other drugs against hypertension, cancer, and diabetes, so it can be characterized as a poly-dynamic drug (Figure 1). (Nakano et al., 2016; Boccellino et al., 2018; Cheng et al., 2018; Shahin et al., 2018; Wang & Li 2018; Yousif et al., 2018; Zhang et al., 2018)

However, IRB is not the ideal medication, as it is practically insoluble in water and has only 60%–70% bioavailability. To circumvent similar problems of high lipophilicity, several drug delivery systems have been developed. Among them, the formulation of IRB with cyclodextrins (CDs) is a promising approach (Hirlekar & Kadam 2009; Jansook et al., 2015). Drugs belonging to Class II of the Biopharmaceutics Classification System (including IRB; Meruva et al., 2019) exhibit low aqueous solubility and high membrane permeability; therefore, their complexation with CDs enhances their oral bioavailability (Loftsson & Brewster 2010).

Phase solubility studies revealed a 72.5% increase in solubility of IRB upon CD addition in stoichiometry of inclusion complex of 1:1. The dissolution rate of the drug increased when it was included in a complex form and depended on the method (co-evaporation gave the highest dissolution rate) (Hirlekar & Kadam 2009).

Differential scanning calorimetry (DSC) experiments indicated the formation of an amorphous entity and the interaction between IRB and β-cyclodextrin (β-CD) through broadening of the peak in the DSC curve of a co-evaporated sample. The IR spectrum of the inclusion complex confirmed the formation of hydrogen bonds between the carbonyl groups of IRB a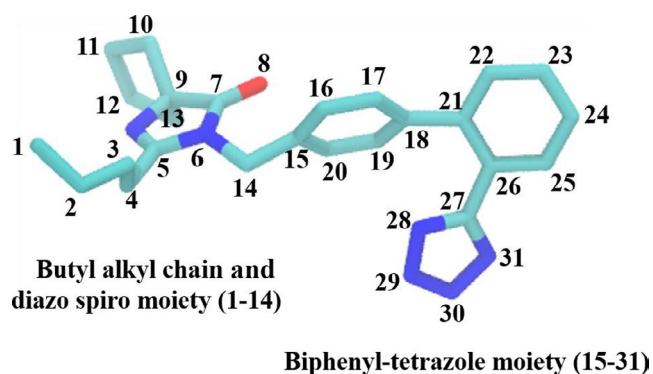nd β-CD during the formation of the inclusion complex. X-ray diffraction data showed that in the inclusion complex the drug was not in a crystalline form in contrast to its non-complexed state. ^{1}H NMR results showed that the extent of inclusion complex formation was comparatively higher than the association of drug with β-CD (Hirlekar & Kadam 2009).

Using FT-IR and ^{1}H NMR spectra, irbesartan was shown to form stable complexes also with γ-CD. The powder diffraction pattern of the hydrophilized IRB/γ-CD confirmed the IRB complex and IRB to be converted from the crystalline to another form. The ionized IRB has greater tendency to form aggregates although it has lower affinity for the hydrophobic γ-CD cavity. Transmission electron microscopy (TEM) analysis provided evidence of IRB/γ-CD complex aggregates (Muankaew et al., 2014).

A recent study examined the effect of pH on the complexation of IRB with β-, hydroxypropyl-β- (HP-β-), and γ-CD by means of solubility enhancement (Yousef 2018). It was reported that IRB achieved the highest solubility when complexed with HP-β-CD at pH = 4.1.

The interactions of IRB–HP-β-CD complex with dipalmitoyl phosphatidylcholine (DPPC) bilayers have been explored utilizing an array of biophysical techniques ranging from DSC, small angle X-ray scattering (SAXS), ESI mass spectrometry (ESI-MS), and solid-state nuclear magnetic resonance (ssNMR). IRB was incorporated in the lipid membrane core and affected the phase transition properties of the DPPC bilayers. SAXS studies revealed that IRB alone does not display perfect solvation as some coexisting IRB crystallites are present. However, in its complexed form, IRB gets fully solvated in the membranes showing that IRB encapsulation in HP-β-CD may have beneficial effects in the ADME properties (Liossi et al., 2017).

Herein, we have sought to synthesize and elucidate the mechanism of action in the complex of irbesartan with 2-HP-β-CD using MS and DSC studies. Importantly, complex formation was predicted through molecular dynamics (MD) simulations, which suggested a spontaneous association of IRB with 2-HP-β-CD. As the complex was foreseen to be stable, it was further subjected to *in vitro* studies. The *in vitro* results are highly promising as they showed that the complexed form is at least equipotent to the drug alone. This encourages additional studies on drug formulations in order to optimize irbesartan's pharmacological properties.

Butyl alkyl chain and diazo spiro moiety (1-14)

Biphenyl-tetrazole moiety (15-31)

FIGURE 1 Chemical structure of irbesartan. Atom numbering corresponds to those mentioned in the MD calculations. Hydrogen atoms are omitted for simplicity [Colour figure can be viewed at wileyonlinelibrary.com]

2 | METHODS AND MATERIALS

2.1 | Preparation of the complex

6783.62 mg of 2-HP-β-CD was transferred in a glass vessel with 800 ml of purified water and set under magnetic stirring. When cyclodextrin was totally dissolved, 1,000 mg of IRB (kindly donated by Prof. M. Koupparis) was added in the

vessel and magnetic stirring was continued. pH was adjusted at approximately 10.5 with NH_3 (5 N), and the reaction of enclosure took place. When the solution was clear, the final volume was fixed at 1,000 ml with purified water and the solution of the complex was immediately frozen at –80°C for lyophilization to follow.

2.2 | Solubility study

The solubility of IRB in various buffers was measured using the shake flask method in a shaking bath apparatus. An excess amount of IRB was introduced into 10 ml of each buffer, and the mixture was kept in sealed conical flasks. Sealed flasks were stirred in a water bath at 37°C for 24 and 48 hr. Samples were filtered to remove the undissolved IRB (0.45 μm), and the filtrate was measured with the HPLC-PDA method described hereunder. The experiment was repeated in triplicate, and the results represent the mean solubility value (mg/ml $\pm$ *SD*). IRB complex with 2-HP-β-CD was completely soluble in excessive amounts of buffers at $t = 0$, and it was considered freely soluble in order to undergo a complete phase solubility study.

2.3 | Fluorescence spectroscopic studies

The binding constant (K_c) of the IRB and 2-HP-β-CD complexation was estimated through steady-state fluorescence spectroscopy. Fluorescence spectra were recorded in a Perkin Elmer LS-55 spectrofluorometer, where the alterations in the IRB fluorescence were examined upon addition of increasing 2-HP-β-CD concentrations. The excitation and emission wavelengths were set to 265 and 370 nm, respectively, and the slits were 10 nm. All measurements were conducted at ambient temperature, using a Quartz (1 cm) cuvette. Stock solutions of IRB (100 μM) and 2-HP-β-CD (12 mM) were prepared in DMSO and dH_2O, respectively. A small volume of the IRB stock solution was mixed each time with increasing volumes of 2-HP-β-CD. For each sample, the final IRB concentration was fixed at 100 μM while various volumes from the 2-HP-β-CD stock solution were added each time (1, 2, 3, 4, 5, and 6 mM). Finally, the samples were adjusted to 3 ml final volume with dH_2O, as needed and left under continuous stirring and protected from light for 30 min.

2.4 | Capsules containing the IRB–2-HP-β-CD complex

For the dissolution rate experiment, the lyophilized complex was weighed and transferred into capsules that served

as pharmaceutical dosage form. The quantity of the complex weighed was calculated in a way that it corresponds to 75 mg of pure IRB (same as the marketed tablet, LUCIDEL©—Elpen Pharmaceuticals), taking into account the final weight of the lyophilized product. In our case, the total amount of complex was approximately 7 g and the quantity corresponding to 75 mg of IRB was 500 mg of complex.

2.5 | Dissolution rate study

The apparatus used was the Erweka DT12 dissolution tester. Each vessel was filled with 500 ml of buffer solution of each pH (3 samples per pH), and the temperature was kept at 37°C with a water circulator and heater. The analysis took place at 100 rpm, and samples were collected at selected time-points (5, 10, 15, 20, 30, 45, 60, 120, and 180 min), taking into account that it is an immediate drug release pharmaceutical form. In every time-point, 2.5 ml of sample was withdrawn and the volume was fixed again at 500 mL by adding 2.5 mL of the same buffer kept also at 37°C. LUCIDEL© tablets were transferred in the vessels as they were, and the complex capsules were put into sinkers in order to avoid floating, while the paddle was rotating. All samples were properly handled (filtered and diluted in HPLC mobile phase if necessary) and directly analyzed onto the HPLC-PDA system.

2.6 | Visual observation

The tablets remained partially undiluted at pH 6.8 and 4.5 for 3 hr, whereas the tablets at pH 1.2 almost immediately disintegrated. The IRB complex capsules were immediately dissolved at pH 1.2, whereas at pH 4.5 and 6.8 there was partial dissolution.

2.7 | HPLC-PDA analysis

The analysis was performed on a Shimadzu HPLC-PDA using a BDS Hypersil 150 × 4.6 mm, 5 μm column. The mobile phase consisted of ACN–sodium acetate buffer pH 3 at a ratio of 55–45. The flow was set at 1.0 ml/min, and IRB was identified at $\lambda_{max} = 260$ nm. The injection volume was 20 μl and the injection time 10 min. A calibration curve was constructed at a range of 0.1–60 μg/ml using pure IRB as a stock solution (initial c = 3 mg/ml). The IRB peak was well separated from other endogenous or solvent peaks, and the elution time was approximately 3.5 min. The HPLC analysis was based on the method of Raja et al. (2012).

2.8 | HR-ESI-MS

The analysis and identification of IRB, 2-HP-β-CD, and their complex IRB–2-HP-β-CD were performed utilizing a hybrid quadrupole time-of-flight (QTOF) mass spectrometer (Maxis Impact, Bruker Daltonics). The QTOF system was equipped with an electrospray ionization interface (ESI), operating in negative ionization mode, with the following operation parameters: capillary voltage 4,000 V; end plate offset, −800 V; nebulizer pressure 0.8 bar; drying gas 4 L/min; and dry gas temperature 180°C. The QTOF MS system operated in full scan acquisition mode and recorded spectra over the *m/z* range 50−3,000, with a scan rate of 1Hz. External calibration of the mass spectrometer was performed with the manufacturer's solution (sodium formate clusters), ensuring high mass accuracy. Stock solutions of 1 mg/ml were prepared for CAN−2-HP-β-CD and CC−2-HP-β-CD complexes, by dissolving the appropriate amounts in water. Preliminary experiments regarding the effect of dissolution solvent highlighted that dissolution of both complexes in either methanol or a mixture of methanol and water 50:50 provided worse results compared to water. Working solutions of 0.01 mg/ml were prepared and used for the infusion experiments. Infusion of the complexes' solutions was performed under a constant flow of 180 µl/min. Identification relied on the mass accuracy of the pseudomolecular ion of each complex, as well as on the conformity of fit between measured and theoretical isotopic pattern. The potential formation of multi-charged species was taken into consideration as well, due to the structure and the high molecular weight (M.W.) of the complexes.

2.9 | Differential scanning calorimetry

The DSC thermograms of IRB, 2-HP-β-CD, different mixtures, and complex of the drug with cyclodextrin were obtained with a DSC822^e Mettler Toledo calorimeter (Schwerzenbach, Switzerland), calibrated with pure indium ($T_m = 156.6$°C). 2-HP-β-CD was analyzed in two different forms, as raw and lyophilized material. The molecule was heated in its raw form, after mechanical mixing and grinding with the raw material or lyophilized cyclodextrin and after complexation with cyclodextrin through lyophilization. For the analysis, approximately 3 mg of dry powder of each sample was weighed in a 40 µl crucible, which was then sealed and left for 15 min to equilibrate. Afterward, each analysis included a 5 min isotherm at 10°C and a heating process from 10 to 300°C, with a heating rate of 10°C/min. The calorimetric data obtained (characteristic transition temperatures T_{onset} and T, enthalpy change ΔH, and width at half peak height of the C_p profiles $\Delta T_{1/2}$) were analyzed using the Mettler Toledo STAR^e software. The transition enthalpy was considered positive during an endothermic process.

2.10 | Molecular modeling

2.10.1 | Structures preparation and molecular docking

The crystal structures of IRB and β-CD were retrieved from the Cambridge Structural Database (CCDC and CSD reference codes: 130127 and BUVSEQ02, respectively). The structure of β-CD was converted to 2-HP-β-CD using Schrödinger 2015.2 (2015)[1]. IRB was initially docked into the interior of 2-HP-β-CD in two most probable orientations (Figure 2) with UCSF DOCK6 (Lang et al., 2009). Next, the two IRB–2-HP-β-CD complexes were subjected to molecular dynamics (MD) simulations.

2.10.2 | Molecular dynamics

The MD calculations were performed with the GPU version of PMEMD (Salomon-Ferrer et al., 2013) from the AMBER16 simulation software[2]. The structure of IRB was geometrically optimized at the HF/6-31G* level with Gaussian 09.[3] Subsequently, RESP charges were generated (Bayly et al., 1993; Wang et al., 2004a) for IRB and the general AMBER force field (GAFF) was employed to assign force field parameters (Wang et al., 2004b). GAFF
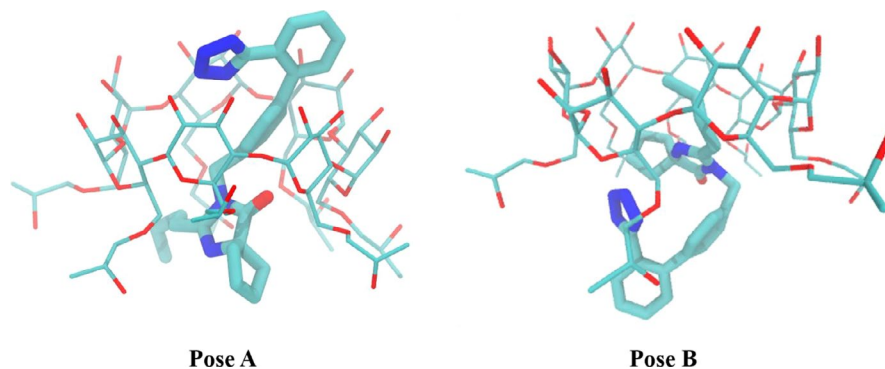
FIGURE 2 The two favored orientations of irbesartan into 2-HP-β-CD as obtained by molecular docking calculations. Hydrogen atoms are not displayed for a simplified representation [Colour figure can be viewed at wileyonlinelibrary.com]

Pose A   **Pose B**

was also used to represent the behavior of the 2-hydroxy-propyl groups of 2-HP-β-CD while the cyclodextrin part was treated with the GLYCAM_06j-1 force field (Kirschner et al., 2008). RESP charges were generated for all atoms of the modified cyclodextrin. Next, each IRB–2-HP-β-CD complex was explicitly solvated in a truncated octahedron containing ~3,600 TIP3P water molecules. (Jorgensen et al., 1983) The minimum distance between each complex atom and the edge of the periodic box was set at 16 Å. IRB complexes were minimized for 30,000 steps, applying a nonbonded cutoff of 10 Å under constant volume. Then, the complexes were gradually heated from 0 to 310 K using a Langevin thermostat (Izaguirre et al., 2001) under constant volume for 400 ps; a collision frequency (γ) of 2/ps was considered. Positional restraints of 10 kcal mol^{-1} Å^{-2} were applied to the atoms of each complex. Next, the constant-pressure equilibration of the systems was obtained in two steps of 400 ps each. In the first step, constraints of 10 kcal mol^{-1} Å^{-2} were applied to the complexes, before all restraints were removed during the final step. Two all-atom, unrestrained MD calculations for IRB in the preferred binding orientations were carried out at 310 K under constant pressure and for 1.2 μs each. During MD, the SHAKE algorithm (Ryckaert et al., 1977) was used to constrain all bonds involving hydrogen atoms close to their equilibrium distance. Analysis of the resulting trajectories was performed with the *cpptraj* module (Roe & Cheatham 2013) of AMBER. Free energy calculations were performed with the molecular mechanics Poisson–Boltzmann surface area (MM–PBSA) method (Kollman et al., 2000; Wang & Kollman 2001; Gohlke et al., 2003); details on the methodology can be found in our previous publications (Kellici, Ntountaniotis, et al., 2015; Kellici, Chatziathanasiadou, et al., 2016).

2.11 | Pharmacological evaluation

Human embryonic kidney (HEK 293) cells stably expressing the human AT1 receptor were grown in DMEM/F12 (1:1) containing 3.15 g/L glucose and 10% bovine calf serum at 37°C and 5% CO_2. Cells at 100% confluence in 100-mm dishes were washed with phosphate-buffered saline (PBS; 4.3 mM $Na_2HPO_4.7H_2O$, 1.4 mM KH_2PO_4, 137 mM NaCl, 2.7 mM KCl, pH 7.2–7.3 at room temperature), briefly treated with PBS containing 2 mM EDTA (PBS/EDTA), and then dissociated in PBS/EDTA. Cell suspension was centrifuged at 1,000×*g* for 5 min at room temperature, and the pellet was homogenized in buffer O (50 mM Tris–HCl containing 0.5 mM EDTA, 10% sucrose, 10 mM $MgCl_2$, pH 7.4 at 4°C) using a Janke & Kunkel IKA Ulra Turrax T25 homogenizer (at setting ~ 20, 10–15 s, 4°C). The homogenate was centrifuged at 250×*g* for 5 min at room temperature. The pellet was discarded, and the supernatant was centrifuged (16,000×*g*,

10 min, 4°C). The membrane pellet was resuspended (0.5–0.6 ml/100 mm dish) in buffer B (50 mM Tris–HCl containing 1 mM EDTA, 10 mM $MgCl_2$, 0.2% BSA, 0.2 mg/ml bacitracin, and 0.93 μg/ml aprotinin, pH 7.4 at 4°C) and used for radioligand binding studies.

Aliquots of membrane suspension (50 μl) were added into tubes, containing buffer B and 90,000–110,000 cpm [^{125}I-Sar^1-Ile^8] AngII without or with increasing concentrations of IRB or IRB–2-HP-β-CD (heterologous competition binding) or increasing concentrations of [Sar^1-Ile^8] AngII (homologous competition binding) in a final volume of 0.15 ml. The mixtures were incubated (1 hr, 24°C) and then filtered using a Brandel cell harvester through Whatman GF/C glass fiber filters, presoaked for 1 hr in 0.5% polyethylenimine at 4°C. The filters were washed 10 times with 1–2 ml of ice-cold 50 mM Tris–HCl containing NaCl 120 mM, pH 7.4 at 4°C. Filters were assessed for radioactivity in a gamma-counter (LKB Wallac 1275 minigamma, 80% efficiency). The amount of membranes used was adjusted to ensure that specific binding was always equal to or <10% of the total concentration of the radioligand added. Specific [^{125}I-Sar^1-Ile^8] AngII binding was defined as the total binding less non-specific binding in the presence of 1,000 nM valsartan. Data for competition binding were analyzed by nonlinear regression analysis, using Prism 4.0 (GraphPad Software). IC_{50} values were obtained by fitting the data from competition studies to a one-site competition model. The binding affinities (K_i or –logK_i values) of AngII analogs were determined from heterologous competition data using GraphPad Prism 4.0 and the equation, $K_i = IC_{50} / (1 + L / K_D)$, where L is the concentration of radioligand (Cheng & Prusoff 1973). The binding affinity (K_D or –logK_D values) of [^{125}I-Sar^1-Ile^8] AngII was determined from homologous competition data, using GraphPad Prism 4.0 and the following equation: Y = {(Bmax * [hot]) / ([hot] + [cold] + K_D)} + NSB (Motulsky & Christopoulus 2004), where Y is the total binding of [^{125}I-Sar^1-Ile^8] AngII, NSB is the non-specific binding of the radioligand, Bmax is the total receptor number, [hot] is the concentration of the [^{125}I-Sar^1-Ile^8] AngII, and [cold] is the concentration of the [Sar^1-Ile^8] AngII.

3 | RESULTS AND DISCUSSION

3.1 | Phase solubility study

IRB bulk's solubility was confirmed to be extremely low at 37°C, pH 1.2, 4.5, and 6.8, even after 48 hr of shaking at 50 rpm. IRB complex with 2-HP-β-CD did not undergo any solubility studies in shaking bath as it appeared freely soluble at *t* = 0 in all buffers prepared (pH 1.2, 4.5, 6.8) (>100 mg/10 ml of solvent) at room temperature. The results for bulk IRB are shown in Table 1.

3.2 | Dissolution experiments

Diagrams obtained from the measurement of peak areas for IRB in both complex and reference tablet are presented below (Figure 3). Both pharmaceutical forms (tablet and lyophilized complex) are less dissolved at pH 4.5 and 6.8, showing that they have not reached the plateau of dissolution. At pH 1.2, the lyophilized complex has a higher dissolution rate than the marketed tablet.

3.3 | HR-ESI-MS

The identification of IRB, 2-HP-β-CD, and IRB–2-HP-β-CD complex was implemented by ESI QTOF HR-ESI-MS analysis. Identification was based on the accurate mass of the pseudomolecular ion ([M-H]$^-$) as well as the conformity between the theoretical and the experimental isotopic profiles. The evaluation of the isotopic pattern fidelity takes into account the mass accuracy and the relative abundance among the isotopes for a given molecular formula. Compounds with high molecular weight have characteristic isotopic patterns, as some of their isotopes share similar intensities with the pseudomolecular monoisotopic ion. Consequently, isotopic profile information provided analytical evidence, especially for the identification of IRB–2-HP-β-CD. Apart from the potential identification of IRB–2-HP-β-CD as a complex, the detection and identification of the drug and 2-HP-β-CD separately were considered as an additional confirmation.

Initial analysis was performed with a method established in a previous study (Ntountaniotis et al., 2019). This method has been developed aiming at molecules with similar molecular weight to IRB–2-HP-β-CD, specifically, for the analysis of candesartan and candesartan cilexitil complexes with 2-HP-β-CD. The ion formation (ESI source) and the ion transfer parameters of MS-based methods are crucial for the sensitivity of the detected ions. Therefore, a fine optimization of these parameters was implemented by focusing on the sensitivity enhancement of IRB–2-HP-β-CD ions. Regarding the optimization procedure, gradual changes of the ion formation and ion transfer parameters were applied while the working solution of

IRB–2-HP-β-CD was infused. The combination of parameters that resulted in the optimum sensitivity for IRB–2-HP-β-CD was used afterward for the identification experiments. The differences of the ion formation and ion transfer parameters before and after optimization are highlighted in Figures S1 and S2 respectively. It is noteworthy that slight changes in the aforementioned parameters resulted in a significant improvement of the sensitivity of IRB–2-HP-β-CD. This becomes obvious in Figure S3 where the [M-H]$^-$ ions of IRB–2-HP-β-CD complex are depicted before (Figure S3a) and after (Figure S3b) the optimization procedure. The sensitivity of IRB–2-HP-β-CD complex was fivefold higher with the optimized method.

A broad distribution of peaks is expected for 2-HP-β-CD in ESI-MS (de Paula et al., 2011; Ntountaniotis et al., 2019), given that 2-HP-β-CD exists as a mixture of CDs with differing degree of substitution by the 2-HP group. Our results concerning the identification of 2-HP-β-CD (Figure
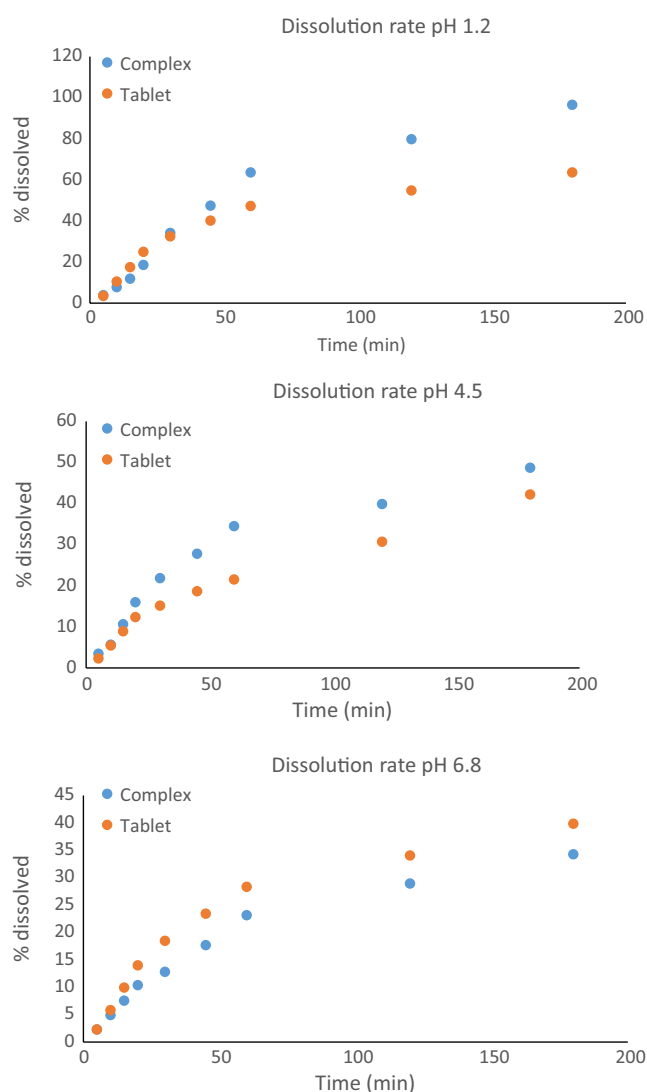

FIGURE 3 Dissolution of tablet and lyophilized complex using pHs 1.2, 4.5, and 6.8 (Error bars not shown since in all cases RSD<2.5%) [Colour figure can be viewed at wileyonlinelibrary.com]

TABLE 1 Solubility results for bulk irbesartan in three buffers of pH 1.2, 4.5, and 6.8

Media of dispersion	Solubility (mg/ml) ± SD—24 hr	Solubility (mg/ml) ± SD—48 hr
pH 1.2 (HCl buffer)	0.09 ± 0.003	0.10 ± 0.004
pH 4.5 (acetate buffer)	0.04 ± 0.001	0.06 ± 0.003
pH 6.8 (phosphate buffer)	0.06 ± 0.003	0.07 ± 0.005

4) comply with data reported in the literature (de Paula et al., 2011; Ntountaniotis et al., 2019). Figure 4a shows the mass spectrum of IRB–2-HP-β-CD solution in the range of 1,200–1,700 Da. The broad distribution of ions corresponds to the pseudomolecular ions of CDs substituted by 2 up to 9 groups of 2-HP (substitution degree: 0.3–1.3). Therefore, 2-HP-β-CD complexes of different substitution degree were identified based on accurate mass measurements and isotopic profile information. Based on our previous results (Ntountaniotis et al., 2019), CDs may form multi-charged species due to their structure characteristics and high M.W. The broad distribution of ions detected in the mass range of 600–850 Da corresponds to the double-charged ions of CDs (Figure 4b). Identification of the uncomplexed drug in the IRB–2-HP-β-CD solution was also achieved through mass accuracy and isotopic profile information. In Figure S4 (a1), the full scan MS spectrum of IRB is presented. Figure S4 (a2), (a3) depicts an overlay of the theoretical and the experimental spectra for [M-H]⁻ and [2M-H]⁻ (dimer) ions of IRB, respectively. There is an excellent fit between the experimental and the theoretical mass spectra, enhancing the identification confidence. It is noted that the formation of IRB dimer ([2M-H]⁻) was concentration-dependent, which was assessed by the infusion of IRB–2-HP-β-CD solutions of differing concentrations.

Regarding the identification of IRB–2-HP-β-CD, a broad distribution of peaks was also expected as IRB forms complexes with CDs with differing degrees of substitution by 2-HP group. In Figure 5, the full scan MS spectrum of IRB–2-HP-β-CD is presented, in the mass range of 1,600–2,150 Da. The ions inside the green rectangles correspond to [M-H]⁻ of IRB–2-HP-β-CD complexes with different substitution degree of β-CD by the 2-HP group. The mass accuracy as well as the isotopic profile of these ions is in accordance with the theoretical ones of IRB–2-HP-β-CD complexes. 2-HP-β-CD can exist in different degrees of substitution, which may occur at different places. In Figure 6, two representative substitutions are shown, namely the 3(2-HP-β-CD) and 4(2-HP-β-CD). Both of them differ by a M.W. of 59. The MS spectra of the complex showed all possible substitutions, taking into account the M.W. of IRB. This becomes evident in Figure 7, where the identification results for the four most intense complexes (5- up to 8-substituted) are depicted, through the overlay of the theoretical and the experimental mass spectra, which are almost identical.

A detailed comparison between the theoretical and experimental spectra for all IRB–2-HP-β-CD complexes (3- up to 9-substituted) is shown in Figure S5. All identification results are presented and explained according to the different degree of complexing of the different complexes. Thus, ESI HRMS analyses resulted in the successful and high-confidence identification of IRB–2-HP-β-CD as well as 2-HP-β-CD and IRB, separately.

3.4 | Determination of the IRB–2-HP-β-CD complex binding constant through fluorescence spectroscopy

Upon incorporation of IRB to cyclodextrin cavity, the spectroscopic properties of the guest molecule may be modified. (Oana et al., 2002; Matei et al., 2007) In a former work, where the interaction of candesartan cilexetil and 2-HP-β-CD was investigated, the fluorescence intensity of the drug was increased with the addition of CD. (Ntountaniotis et al., 2019) The same phenomenon was also observed for the IRB–2-HP-β-CD interaction. When different solutions of 2-HP-β-CD increasing concentrations (1, 2, 3, 4, 5, 6 mM) were added to IRB solution (100 μM), the drug's fluorescence intensity at the maximum wavelength (375 nm) was gradually enhanced (Figure 8a). Taking advantage of the changes in the fluorescence intensity of the drug, we calculated the binding constant of the interaction. The obtained data were plotted in a double reciprocal plot (Figure 8b), followed by linear fitting, and the binding constant was estimated according to the Benesi–Hildebrand equation:

$$\frac{1}{\Delta F} = \frac{1}{\Delta F_c} + \frac{1}{K_c \times \Delta F_c \times [CD]_0} \tag{1}$$

ΔF is the difference between fluorescence intensities in the absence and presence of CD, K_c is the binding constant, ΔF_c describes the difference on intensity between the free and encapsulated forms of IRB at 1:1 molar ratio, and [CD] is the concentration of 2-HP-β-CD. (Alvarez-Parrilla et al., 2005) K_c was calculated to be 503 ± 90/M, suggesting a moderate affinity between IRB and 2-HP-β-CD. This is consistent with the majority of the binding constants determined for similar complexes that are in the range between 10 and 2,000/M. (Loftsson & Brewster 2010) Finally, the straight line of the double reciprocal plot agrees with the HR-ESI-MS results pointing out an 1:1 stoichiometry.

3.5 | Differential scanning calorimetry

The thermodynamic behavior of 2-HP-β-CD in raw material and lyophilized form, as well as of IRB, was assessed. Two types of mixture and the complex of the drug with cyclodextrin were also analyzed and compared with the reference 2-HP-β-CD and IRB thermodynamic profiles. Calorimetric profiles for all materials and systems are shown in Figure 9, and the corresponding thermodynamic parameters are presented in Table 2. As the molar ratio of 2-HP-β-CD:IRB is 1:1 and the weight ratio is close to 3.6:1, the % amount of the drug is 21.74%. This is useful to roughly estimate the amount of drug encapsulated
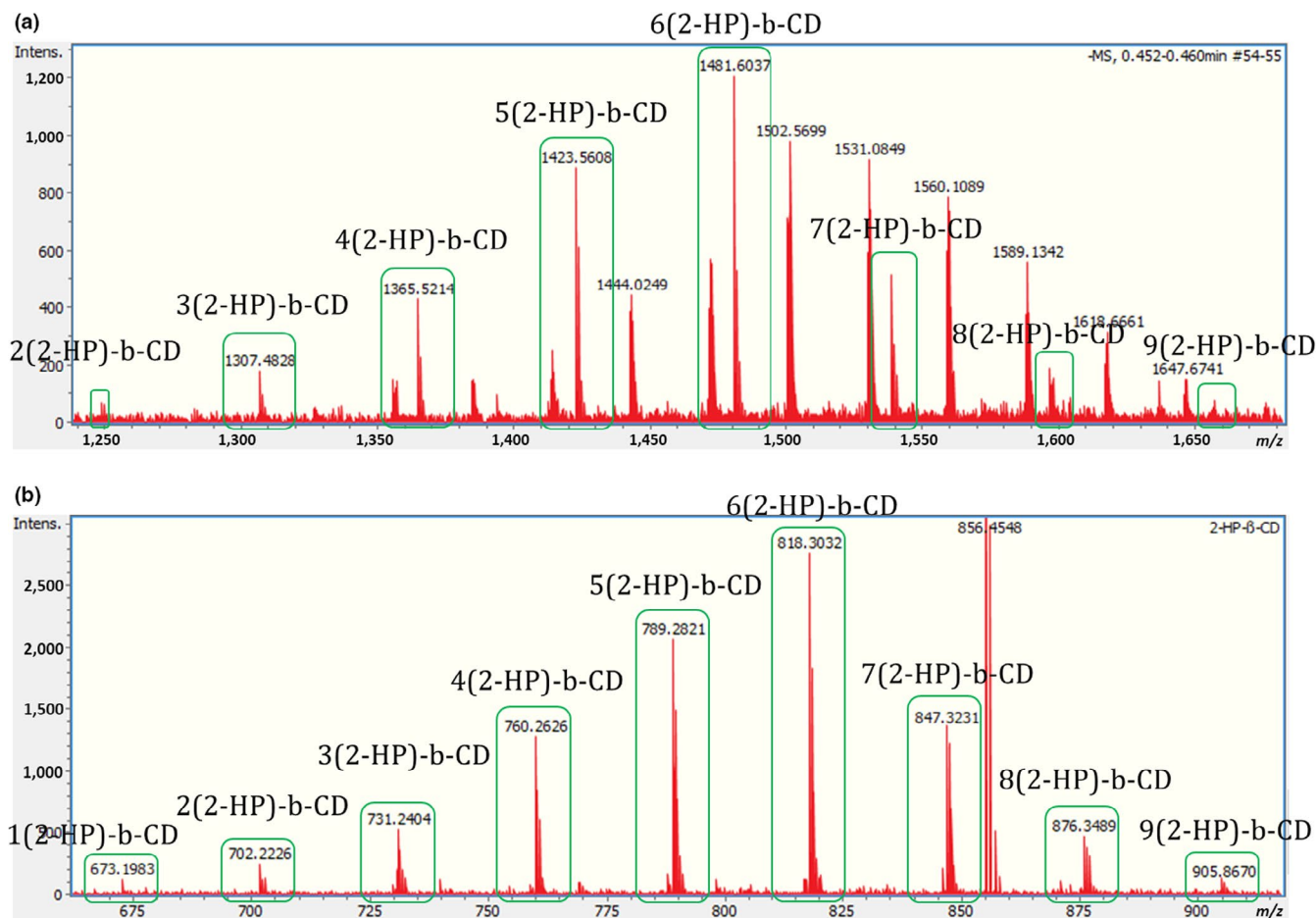
FIGURE 4 (a) Mass spectrum of IRB–2-HP-β-CD solution, in the range of 1,200–1,700 Da, encompassing the single-charged ions of cyclodextrins substituted by 2 up to 9 groups of 2-HP, and (b) mass spectrum of the same solution, in the range of 600–850 Da, encompassing the double-charged ions of cyclodextrins substituted by 1 up to 9 groups of 2-HP [Colour figure can be viewed at wileyonlinelibrary.com]
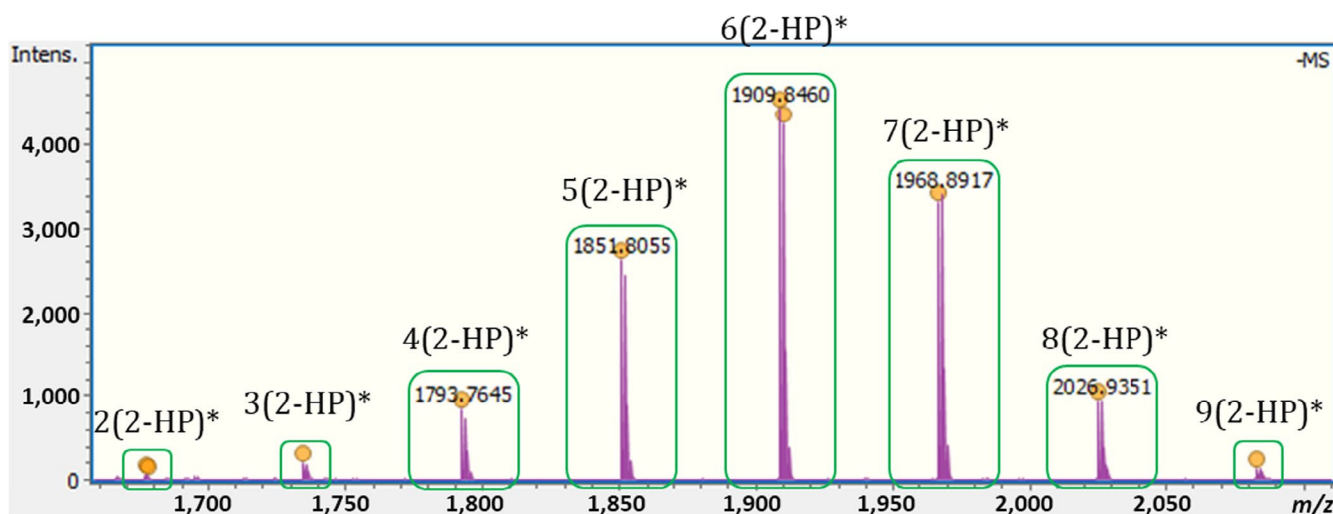

FIGURE 5 Full scan MS spectrum of IRB–2-HP-β-CD in the mass range of 1,600–2,150 Da. The ions inside the green rectangles correspond to [M-H]⁻ ions of IRB–2-HP-β-CD complexes with different substitution degree of β-CD by 2-HP group. The asterisk represents IRB–2HP-β-CD [Colour figure can be viewed at wileyonlinelibrary.com]

in each case of mixture or complex with 2-HP-β-CD. In addition, each mixture was compared with either raw material or lyophilized CD, depending on the included form of CD, while the complex was compared with the lyophilized form, because of the correspondence in preparation methodology.
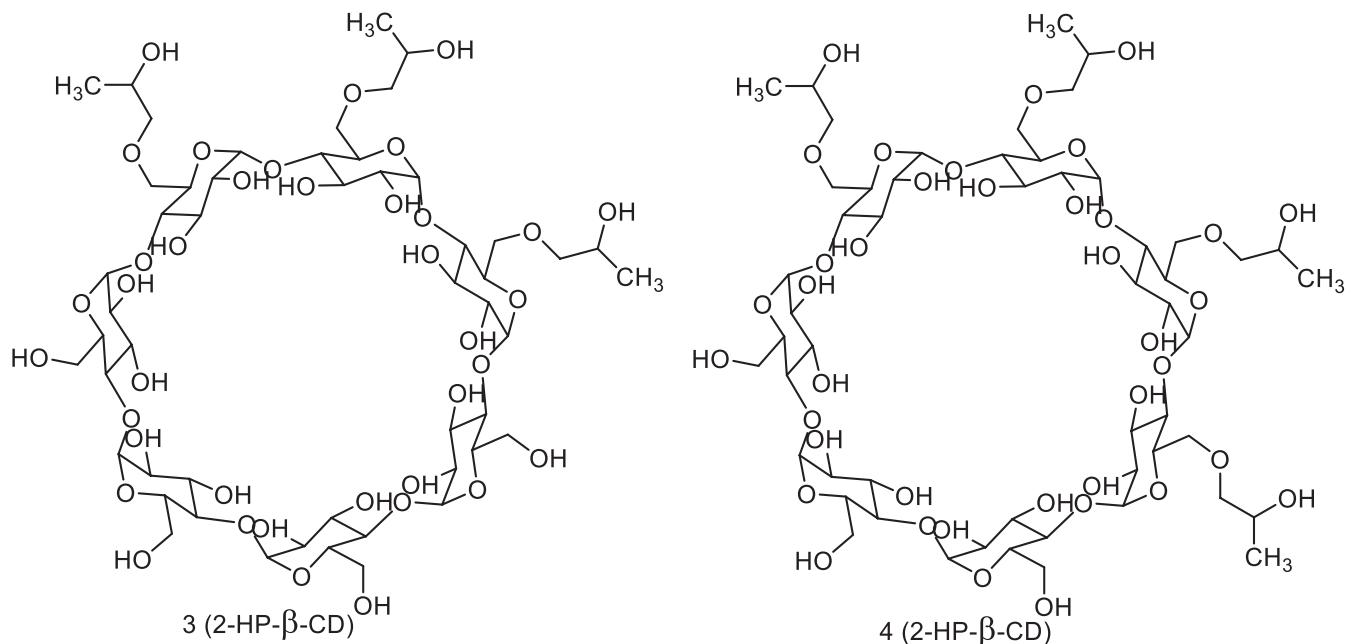
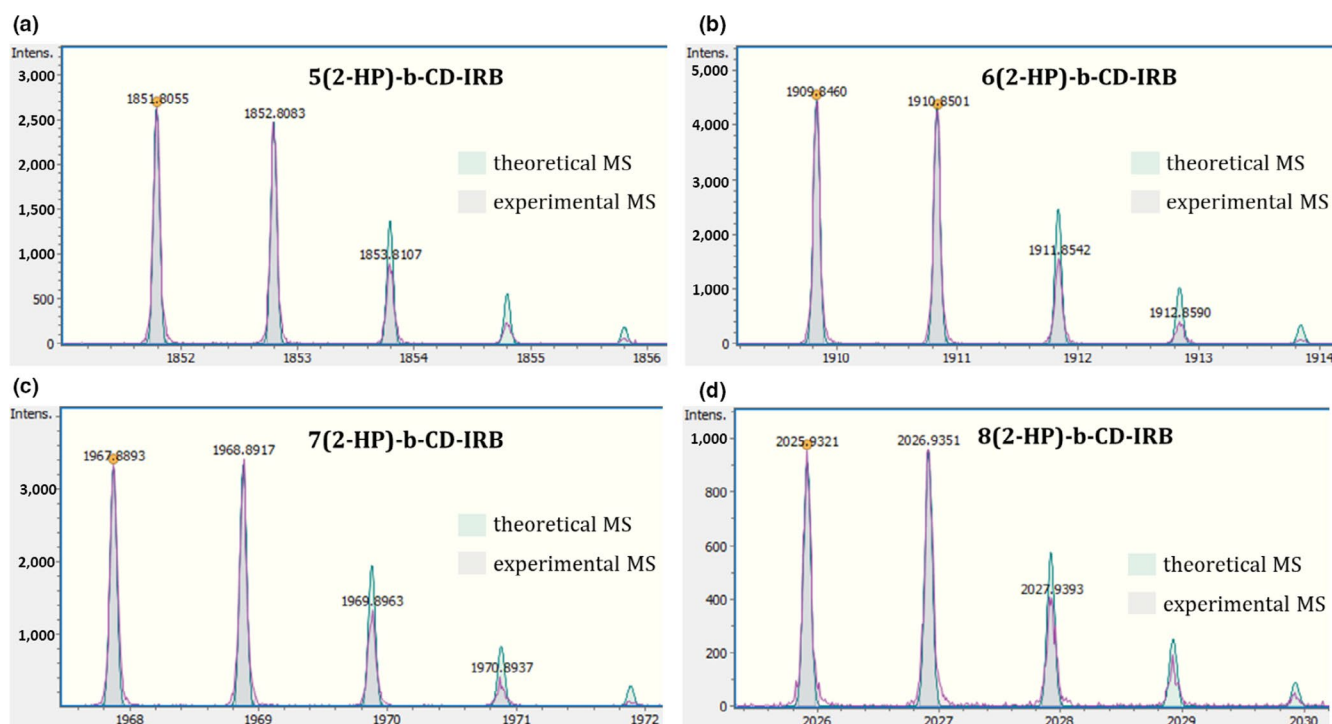**FIGURE 6** Two representative structures of 3(2-HP-β-CD) and 4(2-HP-β-CD)

FIGURE 7 Overlay of the theoretical and experimental mass spectra for the four most intense complexes (5- up to 8-substituted) of IRB–2-HP-β-CD. High mass accuracy and isotopic fidelity resulted in successful identification [Colour figure can be viewed at wileyonlinelibrary.com]

2-HP-β-CD was analyzed as raw material and after lyophilization. There were no considerable differences between the two cases, apart from the transition width at half peak, which was double for the lyophilized form and indicates loss of crystallinity and broadening of the transition peak as more cycles of lyophilization take place. The other parameters were similar, with the transition peak temperature being around 168–170°C. The transition enthalpy was also slightly lower for the lyophilized form. These sharp transitions indicate that CD is more crystalline and less amorphous, compared with other studies, and melts at a very narrow temperature range (Kratz et al., 2012). A case of M-β-CD has been documented, where a sharp transition was observed at 158°C, similar to our 2-HP-β-CD (Soares da Silva et al., 2011).
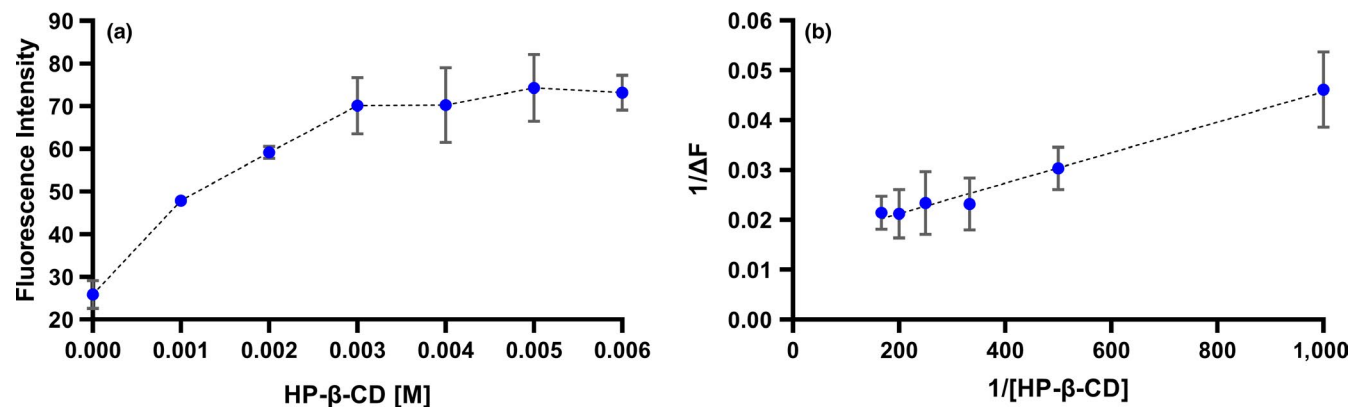
FIGURE 8   (a) Fluorescence intensities of IRB at 375 nm upon addition of different 2-HP-β-CD concentrations. (b) Double reciprocal plot of the fluorescence intensity difference between the complexed and free IRB against the reciprocal concentration of 2-HP-β-CD. The occurred data represent the average of three independent experiments [Colour figure can be viewed at wileyonlinelibrary.com]
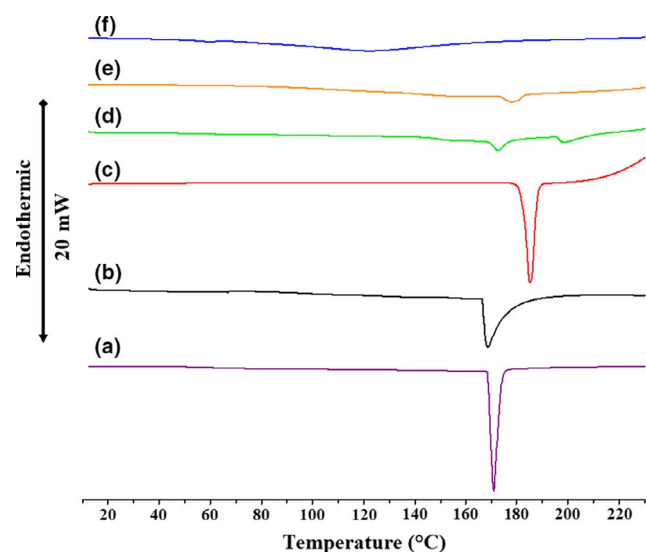

FIGURE 9   DSC curves of (a) raw material 2-HP-β-CD, (b) lyophilized 2-HP-β-CD, (c) irbesartan, (d) mixture of the drug with raw material 2-HP-β-CD, (e) mixture of the drug with lyophilized 2-HP-β-CD, and (f) lyophilized complex of the drug with 2-HP-β-CD. The bar represents a heat flow amount of 20 mW [Colour figure can be viewed at wileyonlinelibrary.com]

IRB gave a characteristic melting/endothermic transition peak at 184.63°C, after which decomposition occured. The thermogram and calorimetric values were close to those documented in the literature (Soma et al., 2017). The transition enthalpy is very important, because the comparison with the mixture and complex with 2-HP-β-CD offers an estimation of the amount of drug encorporated inside cyclodextrin.

When mixed or complexed with 2-HP-β-CD, IRB behaves differently. The heating curves of 2-HP-β-CD:IRB mixtures and complex are provided in Figure 10. Raw 2-HP-β-CD:IRB mixture began to melt at very low temperature, but the heat absorption was low and became significant above 140°C, with the first peak appearing at 172.57°C (attributed to CD), while the second one at 198.60°C (probably IRB). If the two peak transition enthalpies are normalized per 2-HP-β-CD (78.26% of sample size) and IRB (21.74% of sample size) amounts, they each give around half the energy compared with free raw material CD (55.21 vs. 90.53 J/g) and free drug (44.43 vs. 95.38 J/g). Thus, we assume that at least half the amount of IRB is left unencapsulated, although it may be more than that, as the baselines for these calculations ignore a significant amount of enthalpy and a segment of the drug transition may be hidden inside the whole transition. The total transition enthalpy of the whole area under the curve normalized per total sample (176.72 J/g) is close to the transition enthalpy of the whole area of raw CD (179.32 J/g). This means that the system between drug and CD absorbs the same amount of energy with neat CD in order to melt, including the amount of energy absorbed by the crystalline IRB.

On the other hand, when mixed with lyophilized 2-HP-β-CD, IRB interacts differently and to a larger extend with CD. Specifically, the beginning of the endothermic phenomenon at low temperature, the peak onset temperature, and the peak temperature are similar, with the latter being 5.5°C higher (possibly attributed to CD, again). However, a second peak at higher temperature was not observed, meaning that IRB interacts more intensively with the lyophilized CD. This interaction leads 2-HP-β-CD to a higher melting peak, that is, 168-170 °C if alone, 172.57 °C when mixed in a raw material form with the drug, and 178.06 °C when mixed in the lyophilized form. Additionally, the transition enthalpy of the small peak was considerably lower than the previous case of mixture when normalized per cyclodextrin (15.24 J/g vs. 55.21 J/g) and the total transition enthalpy was much higher than before (257.90 J/g vs. 176.72 J/g). The peak width is also larger, and the transition is broader than in the case of mixture with raw CD. These comparisons prove that a higher amount of IRB interacts and is possibly encapsulated when mechanically mixed with lyophilized 2-HP-β-CD, rather than with raw 2-HP-β-CD.

TABLE 2 Thermodynamic parameters of the peaks that appeared during heating of 2-HP-β-CD in raw material and lyophilized form, drug molecules, their mixtures, and complexes

Sample	Molar Ratio	Weight Ratio	T_{onset} (°C)	T (°C)	$\Delta T_{1/2}$ (°C)	ΔH (J/g)
2-HP-β-CD Raw Material	–	–	168.20	169.93	3.01	179.32
2-HP-β-CD Lyophilized	–	–	166.03	168.14	6.69	165.17
Irbesartan	–	–	182.19	184.63	3.50	95.38
Raw 2-HP-β-CD:IRB Mixture	1:1	3.6:1	165.78	172.57	9.32	176.72
1st Peak	–	–	167.31	172.57	5.85	43.21
1st Peak Normalized Per 2-HP-β-CD	–	–	–	–	–	55.21
2nd Peak	–	–	195.62	198.60	7.33	9.66
2nd Peak Normalized Per IRB	–	–	–	–	–	44.43
Lyo 2-HP-β-CD:IRB Mixture	1:1	3.6:1	166.85	178.06	48.61	257.90
Peak	–	–	172.79	178.06	7.04	11.93
Peak Normalized Per 2-HP-β-CD	–	–	–	–	–	15.24
2-HP-β-CD:IRB Complex	1:1	3.6:1	66.43	122.10	65.26	231.69
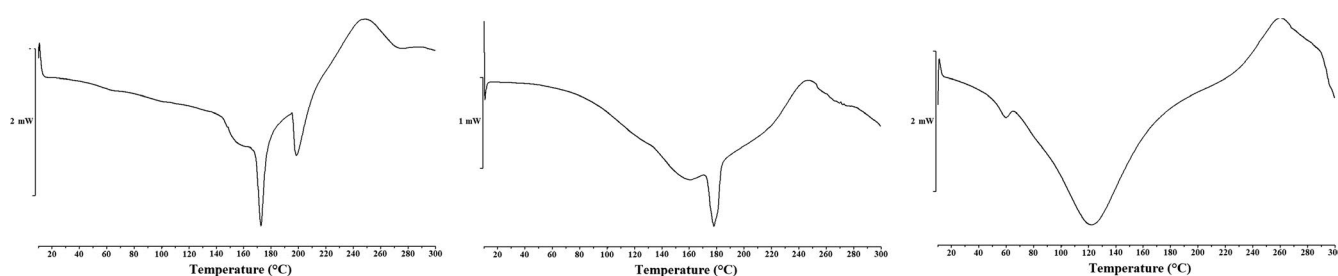
FIGURE 10 Heating profiles of raw material 2-HP-β-CD:IRB mixture (right), lyophilized 2-HP-β-CD:IRB mixture (middle), and 2-HP-β-CD:IRB complex (left)

The 2-HP-β-CD:IRB complex gives a broad endothermic peak, starting at very low temperature and absorbing a high amount of energy, close to the total of lyophilized CD and drug together (231.69 J/g vs. 165.17 and 95.38 J/g). This indicates the high efficacy of encapsulation of the drug into CD, where its physical state is altered from crystalline to amorphous (Khandai et al., 2013). This transition resembles the one of lyophilized 2-HP-β-CD:IRB mixture, in terms of morphology, peak width, and transition enthalpy, yet it differs from the one of raw 2-HP-β-CD:IRB mixture.

Generally, either CD or the drug alone gave sharp peaks, because they were single ingredients, which when mixed together through physical mixing (mixture), or through a complexation process (complex), they interacted and displayed broad peaks. The complex especially is formed by solubilization of the drug inside aqueous medium through complexation and lyophilization. As a result, binding interactions become profound. On the other hand, the mixture involves mixing the two ingredients in crystalline state, where they do not interact extensively. When mixed with lyophilized CD, IRB interacts either through surface phenomena, for example, hydrophobic or encapsulation into 2-HP-β-CD. The above results indicate that the process of bringing together the two ingredients through lyophilization or mechanical mixing is less important than the initial physical state of CD (i.e., raw material or lyophilized), when attempting to build a stable drug–CD complex.

The DSC results agree with those obtained by Yousef using β-CD instead of 2-HP-β-CD (Yousef 2018). IRB showed one endothermic peak at about 181°C in agreement with our data. In the mixture, IRB was still evident but it disappeared in the thermogram of the complex, indicating the formation of IRB–β-CD inclusion complex again, as it is obtained with 2-HP-β-CD.
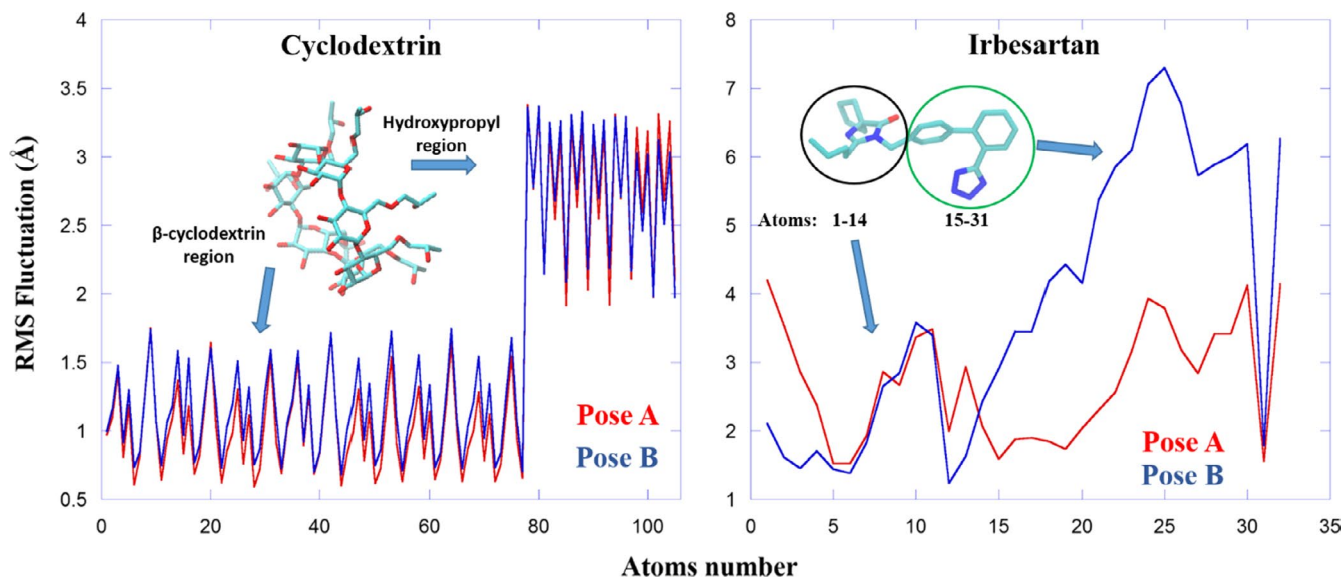
FIGURE 11 Root mean square fluctuations of cyclodextrin and IRB in the two IRB–2-HP-β-CD complexes [Colour figure can be viewed at wileyonlinelibrary.com]

3.6 | Molecular dynamics

Extensive MD simulations for the two different poses of IRB into 2-HP-β-CD (total simulation time 2.4 μs) suggested that the structures of the complexes display similar stability throughout the runs. Particularly, when cyclodextrin binds IRB in either pose A or pose B, it appears significantly stable with RMSD values that fluctuate around an average of ~2.6 Å (Figure S6). Similarly, IRB acquires a stable structure in complexes with 2-HP-β-CD regardless of its initial binding orientation; however, when adopts pose B, the drug appears more flexible compared to pose A (Figure S6, right).

The structural properties of the IRB–2-HP-β-CD complexes were further evaluated by RMS fluctuation calculations as shown in Figure 11. As expected, the β-cyclodextrin part of 2-HP-β-CD is very stable while the hydroxypropyl moieties significantly increase the flexibility of the system (Figure 11, left). Interestingly, the higher flexibility of IRB in pose B as observed by the RMSD calculations above may be attributed to the mobility of the biphenyl tetrazole moiety of the drug (green encircled region, Figure 11). While IRB atoms 1-14 (diazo spiro and butyl alkyl chain) appear equally flexible between the two poses, atoms 15-31 (biphenyltetrazole) significantly increase the molecule's mobility in pose B.

Further binding free energy calculations for the two IRB–2-HP-β-CD complexes revealed the major interactions between IRB and cyclodextrin in each pose. MM–PBSA analysis showed that the binding is driven by enthalpy contributions and, more particularly, through significant van der Waals interactions (Table 3). Despite that electrostatic interactions between IRB and 2-HP-β-CD also contribute favorably, the total electrostatics of the system does not favor

TABLE 3 Energetic analysis for the two IRB complexes with 2-HP-β-CD as obtained by MM–PBSA calculations

Energy (kcal/mol)	Pose A	Pose B
ΔE_{vdW}	-47.22 ± 0.04^a	-45.16 ± 0.05
ΔE_{elec}	-33.27 ± 0.14	-26.67 ± 0.09
$\Delta E_{MM, gas}$	-80.49 ± 0.15	-71.83 ± 0.10
ΔG_{PB}	49.75 ± 0.11	43.52 ± 0.08
$\Delta G_{elec(tot)}{}^b$	16.48 ± 0.14	16.85 ± 0.13
ΔG_{NP}	-4.12 ± 0.00	-4.03 ± 0.00
ΔG_{solv}	45.62 ± 0.11	39.49 ± 0.08
$\Delta H_{(MM+solv)}$	-34.87 ± 0.06	-32.34 ± 0.05
$-T\Delta S_{tot}$	23.29 ± 0.04	22.24 ± 0.05
$\Delta G_{MM-PPSA}$	-11.58 ± 0.11^c	-10.10 ± 0.08^c

[a]Errors represent standard errors of the mean (SEM): SEM = standard deviation / $\sqrt{N}$, where N is the number of trajectory frames used in MM−PBSA calculations (200 for entropy and 10,000 for everything else).

[b]$\Delta G_{elec(tot)} = \Delta E_{elec} + \Delta G_{PB}$.

[c]The error bars for $\Delta G_{MM-PBSA}$ have been estimated as pooled standard errors of the mean based on the formula $S = \sqrt{\frac{(n_1-1)(s_1)^2+(n_2-1)(s_2)^2}{n_1+n_2-2}}$, where n_1 is the number of frames for the ΔH calculation ($n_1 = 10,000$), n_2 is the number of frames for the $-T\Delta S$ calculation ($n_2 = 200$), and s_1 and s_2 are the standard errors of the mean of ΔH and $-T\Delta S$ calculations, respectively.

binding, mainly due to solvent effects. Calculations of the total binding energy ($\Delta G_{MM-PBSA}$) suggested that the drug has an adequate binding affinity for 2-HP-β-CD (~10–11 kcal/mol, Table 3), so that it may be effectively transported by cyclodextrin. At the same time, the predicted binding affinity may not be high enough to prevent eventual release of IRB from its host. Therefore, the hypothesis of 2-HP-β-CD to be an effective IRB carrier should be considered. In this
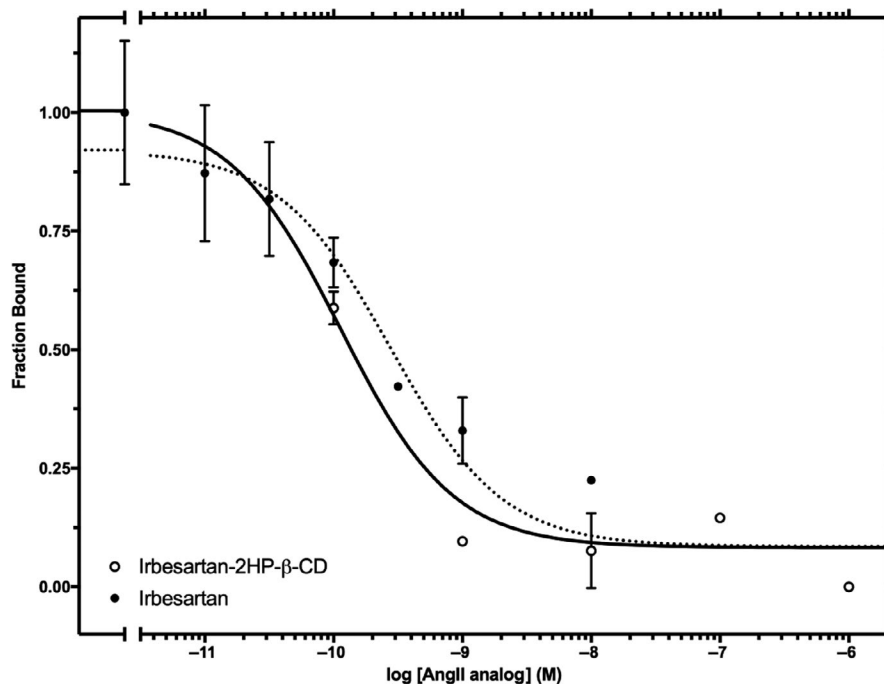
FIGURE 12 Competition binding isotherms of AngII analogs to human AT1 receptor. Competition of $[^{125}\text{I-Sar}^1\text{-Ile}^8]$ AngII specific binding by increasing concentrations of AngII analogs was performed, as described under "Methods and Materials," on membranes from HEK 293 cells stably expressing the human AT1 receptor. The means and S.E. (duplicate determination) are shown from a representative experiment performed 2 times with similar results. The data were fit to a one-site competition model by nonlinear regression. The K_i values were calculated (as described under "Methods and Materials") and are given in the manuscript

way, the greater flexibility of the biphenyltetrazole moiety of IRB when binds in pose B compared to pose A (Figure 9) may facilitate the eventual release of the drug.

3.7 | Pharmacological evaluation

We pharmacologically characterized IRB and IRB–2-HP-β-CD by determining their binding affinities (K_i) for the AT1 receptor in competition binding experiments performed under equilibrium conditions in membranes from HEK 293 cells stably expressing the receptors. As shown in Figure 12, the complexation of IRB to 2-HP-β-CD did not alter the binding properties of compounds. Specifically, the binding affinities of IRB–2-HP-β-CD ($K_i = 0.16 \pm 0.05$ nM; $n = 2$) for the AT1 receptor did not considerably differ from that of IRB ($K_i = 0.36 \pm 0.11$ nM; $n = 2$). The K_i values of IRB and IRB–2-HP-β-CD were determined from their IC_{50} values, which were obtained from heterologous competition data and using the equation: $K_i = IC_{50}/(1 + L/K_D)$, as described in the Methods and Materials (Cheng & Prusoff 1973). The K_D (or $-\log K_D$) value for $[^{125}\text{I-Sar}^1\text{-Ile}^8]$ AngII binding, which was determined from homologous competition data and represents the binding affinity of radioligand, was 1.35 ± 0.13 nM ($n = 2$). Additionally, according to our previous study, 2-HP-β-CD does not bind to human AT1 receptor (Ntountaniotis et al., 2019).

4 | CONCLUSIONS

ESI QTOF HRMAS demonstrated the 1:1 complexation of IRB with the low DS and high DS 2-HP-β-CDs, in agreement

with fluorescence experiments. Dissolution experiments revealed the higher dissolution rate of the complex vs the tablets containing only the bioactive IRB. This is important as the high lipophilic IRB suffers from low dissolution. It was unequivocally shown that DSC thermal scans of a mixture containing IRB and 2-HP-β-CD differed significantly with that of the complex IRB–2-HP-β-CD. Interestingly, the mixture produced a thermal scan that was not the mere addition of the two components; it rather indicated some association between them. This association was stronger when lyophilized 2-HP-β-CD was used and probably also some encapsulation occurred. This is an interesting observation, which has not been reported before, as the thermal properties of the mixtures appear to be totally ignored. Such information signifies that DSC can be also used to study the similarities of different kinds of mixtures with complexes.

MD simulations provided evidence that IRB favors complexation with 2-HP-β-CD in two different ways of approach (poses A and B). In the two poses, the atoms composing the diazo spiro and butyl alkyl chain appear equally flexible, while those of the biphenyl tetrazole are more flexible in pose B.

Pharmacological *in vitro* studies identified the K_i of the complex (0.16 ± 0.05 nM) and of the drug alone (0.36 ± 0.11 nM). This intriguing result indicates that the drug, either alone or after being released from the complex form, may approach equally well the lipid bilayers and reach the active site through the lipid matrix or directly from the receptor extracellular portion. As IRB is highly lipophilic, in a real biological environment it is anticipated to find more obstacles in its way to the AT1 receptor than in the new formulation, which contains the IRB–2-HP-β-CD complex. In agreement with *in vitro* experiments, the Kc calculated

from fluorescence studies was 503 ± 90/M, suggesting a moderate affinity between IRB and 2-HP-β-CD, and therefore easy release of the drug from the hydrophobic cavity of cyclodextrin.

ACKNOWLEDGMENTS

CONFLICT OF INTEREST

The authors have no conflict of interest to declare.

DATA AVAILABILITY STATEMENT

The data that support the findings of this study are available from the corresponding author upon reasonable request.

ORCID

Eirini Christodoulou https://orcid.org/0000-0003-1902-9666
Thomas Mavromoustakos https://orcid.org/0000-0001-5309-992X
Dimitrios E. Damalas https://orcid.org/0000-0002-2997-7566
Nikolaos Naziris https://orcid.org/0000-0002-8155-3875

ENDNOTES

[1] (2015). Schrödinger Release 2015-2: Maestro, Schrödinger, LLC, New York, NY.

[2] D.A. Case, R.M. Betz, D.S. Cerutti, T.E. Cheatham, I., T.A. Darden, R.E. Duke, et al. (2016). AMBER 2016, University of California, San Francisco.

[3] Frisch, M.J.T., G.W.; Schlegel, H. B.; Scuseria, G. E.; Robb, M. A.; Cheeseman, J. R.; Scalmani, G.; Barone, V.;Mennucci, B.; Petersson, G. A.; Nakatsuji, H.; Caricato, M.; Li, X.; Hratchian, H. P.; Izmaylov, A. F.; Bloino, J.; Zheng, G.; Sonnenber, D. J (2009). Gaussian 09. *Gaussian, Inc. Wallingford CT*, 2-3. doi: 111.

REFERENCES

Adams, M. A., & Trudeau, L. (2000). Irbesartan: review of pharmacology and comparative properties. *The Journal of Clinical Pharmacology*, *7*(1), 22–31.

Alvarez-Parrilla, E., Rosa, L. A. D. L., Torres-Rivas, F., Rodrigo-Garcia, J., & González-Aguilar, G. A. (2005). Complexation of apple antioxidants: Chlorogenic acid, quercetin and rutin by β-Cyclodextrin (β-CD). *Journal of Inclusion Phenomena and Macrocyclic Chemistry*, *53*(1), 121–129. https://doi.org/10.1007/s10847-005-1620-z

Bayly, C. I., Cieplak, P., Cornell, W., & Kollman, P. A. (1993). A well-behaved electrostatic potential based method using charge restraints for deriving atomic charges: The RESP model. *The Journal of Physical Chemistry*, *97*(40), 10269–10280. https://doi.org/10.1021/j100142a004

Boccellino, M., Di Domenico, M., Donniacuo, M., Bitti, G., Gritti, G., Ambrosio, P., … Rinaldi, B. (2018). AT1-receptor blockade: Protective effects of irbesartan in cardiomyocytes under hypoxic stress. *PLoS ONE*, *13*(10), e0202297. https://doi.org/10.1371/journal.pone.0202297

Cheng, Y., & Prusoff, W. H. (1973). Relationship between the inhibition constant (K1) and the concentration of inhibitor which causes 50 per cent inhibition (I50) of an enzymatic reaction. *Biochemical Pharmacology*, *22*(23), 3099–3108.

Cheng, Y.-Z., Yang, S.-L., Wang, J.-Y., Ye, M., Zhuo, X.-Y., Wang, L.-T., … Yang, L. I. (2018). Irbesartan attenuates advanced glycation end products-mediated damage in diabetes-associated osteoporosis through the AGEs/RAGE pathway. *Life Sciences*, *205*, 184–192. https://doi.org/10.1016/j.lfs.2018.04.042

de Paula, W. X., Denadai, A. M., Santoro, M. M., Braga, A. N., Santos, R. A., & Sinisterra, R. D. (2011). Supramolecular interactions between losartan and hydroxypropyl-beta-CD: ESI mass-spectrometry, NMR techniques, phase solubility, isothermal titration calorimetry and anti-hypertensive studies. *International Journal of Pharmaceutics*, *404*(1–2), 116–123. https://doi.org/10.1016/j.ijpharm.2010.11.008

Gohlke, H., Kiel, C., & Case, D. A. (2003). Insights into protein-protein binding by binding free energy calculation and free energy decomposition for the Ras-Raf and Ras-RalGDS complexes. *Journal of Molecular Biology*, *330*(4), 891–913. S0022283603006107[pii]

Hirlekar, R., & Kadam, V. (2009). Preformulation study of the inclusion complex irbesartan-beta-cyclodextrin. *An Official Journal of the American Association of Pharmaceutical Scientists*, *10*(1), 276–281. https://doi.org/10.1208/s12249-009-9206-5

Izaguirre, J. A., Catarello, D. P., Wozniak, J. M., & Skeel, R. D. (2001). Langevin stabilization of molecular dynamics. *Journal of Chemical Physics*, *114*(5), 2090–2098. https://doi.org/10.1063/1.1332996

Jansook, P., Muankaew, C., Stefansson, E., & Loftsson, T. (2015). Development of eye drops containing antihypertensive drugs: Formulation of aqueous irbesartan/gammaCD eye drops. *Pharmaceutical Development and Technology*, *20*(5), 626–632. https://doi.org/10.3109/10837450.2014.910811

Jorgensen, W. L., Chandrasekhar, J., Madura, J. D., Impey, R. W., & Klein, M. L. (1983). Comparison of simple potential functions for simulating liquid water. *Journal of Chemical Physics*, *79*(2), 926–935. https://doi.org/10.1063/1.445869

Kellici, T. F., Chatziathanasiadou, M. V., Diamantis, D., Chatzikonstantinou, A. V., Andreadelis, I., Christodoulou, E., … Tzakos, A. G. (2016). Mapping the interactions and bioactivity of quercetin-(2-hydroxypropyl)-beta-cyclodextrin complex. *International Journal of Pharmaceutics*, *511*(1), 303–311. https://doi.org/10.1016/j.ijpharm.2016.07.008

Kellici, T. F., Liapakis, G., Tzakos, A. G., & Mavromoustakos, T. (2015). Pharmaceutical compositions for antihypertensive treatments: A patent review. *Expert Opinion on Therapeutic Patents*, *25*(11), 1305–1317. https://doi.org/10.1517/13543776.2015.1086337

Kellici, T. F., Ntountaniotis, D., Kritsi, E., Zervou, M., Zoumpoulakis, P., Potamitis, C., … Mavromoustakos, T. (2016). Leveraging NMR and X-ray data of the free ligands to build better drugs targeting angiotensin II type 1 G-protein coupled receptor. *Current Medicinal Chemistry*, *23*(1), 36–59.

Kellici, T. F., Ntountaniotis, D., Leonis, G., Chatziathanasiadou, M., Chatzikonstantinou, A. V., Becker-Baldus, J., & Mavromoustakos, T. (2015). Investigation of the interactions of silibinin with 2-hydroxypropyl-beta-cyclodextrin through biophysical techniques and

computational methods. *Molecular Pharmaceutics*, *12*(3), 954–965. https://doi.org/10.1021/mp5008053

Khandai, M., Chakraborty, S., & Ghosh, A. (2013). Losartan potassium loaded bioadhesive micro-matrix system: An investigation on effects of hydrophilic polymeric blend on drug release. *Pharmaceutica Analytica Acta*, *S8*, 001. https://doi.org/10.4172/2153-2435.S8-001

Kirschner, K. N., Yongye, A. B., Tschampel, S. M., González-Outeiriño, J., Daniels, C. R., Foley, B. L., & Woods, R. J. (2008). GLYCAM06: a generalizable biomolecular force field. Carbohydrates. *Journal of Computational Chemistry*, *29*(4), 622–655. https://doi.org/10.1002/jcc.20820

Kollman, P. A., Massova, I., Reyes, C., Kuhn, B., Huo, S., Chong, L., … Cheatham, T. E. (2000). Calculating structures and free energies of complex molecules: combining molecular mechanics and continuum models. *Accounts of Chemical Research*, *33*(12), 889–897. ar000033j[pii].

Kratz, J. M., Teixeira, M. R., Ferronato, K., Teixeira, H. F., Koester, L. S., & Simoes, C. M. (2012). Preparation, characterization, and in vitro intestinal permeability evaluation of thalidomide-hydroxypropyl-beta-cyclodextrin complexes. *An Official Journal of the American Association of Pharmaceutical Scientists*, *13*(1), 118–124. https://doi.org/10.1208/s12249-011-9739-2

Lang, P. T., Brozell, S. R., Mukherjee, S., Pettersen, E. F., Meng, E. C., Thomas, V., … Kuntz, I. D. (2009). DOCK 6: Combining techniques to model RNA-small molecule complexes. *RNA*, *15*(6), 1219–1230. https://doi.org/10.1261/rna.1563609

Liossi, A. S., Ntountaniotis, D., Kellici, T. F., Chatziathanasiadou, M. V., Megariotis, G., Mania, M., … Mavromoustakos, T. (2017). Exploring the interactions of irbesartan and irbesartan-2-hydroxypropyl-beta-cyclodextrin complex with model membranes. *Biochimica Et Biophysica Acta - Biomembranes*, *1859*(6), 1089–1098. https://doi.org/10.1016/j.bbamem.2017.03.003

Loftsson, T., & Brewster, M. E. (2010). Pharmaceutical applications of cyclodextrins: basic science and product development. *Journal of Pharmacy and Pharmacology*, *62*(11), 1607–1621. https://doi.org/10.1111/j.2042-7158.2010.01030.x

Matei, I., Nicolae, A., & Hillebrand, M. (2007). *Fluorimetric and molecular mechanics study of the inclusion complex of 2-quinoxalinyl-phenoxathiin with β -cyclodextrin*.

Meruva, S., Thool, P., Shah, S., Karki, S., Bowen, W., Ghosh, I., & Kumar, S. (2019). Formulation and performance of Irbesartan nanocrystalline suspension and granulated or bead-layered dried powders - Part I. *International Journal of Pharmaceutics*, *568*, 118189. https://doi.org/10.1016/j.ijpharm.2019.03.007

Motulsky, H., & Christopoulus, A. (2004). *Fitting models to biological data using linear and nonlinear regression. A practical guide to curve fitting*. Oxford University Press: GraphPad Software Inc.

Muankaew, C., Jansook, P., Stefansson, E., & Loftsson, T. (2014). Effect of gamma-cyclodextrin on solubilization and complexation of irbesartan: Influence of pH and excipients. *International Journal of Pharmaceutics*, *474*(1–2), 80–90. https://doi.org/10.1016/j.ijpharm.2014.08.013

Nakano, Y., Matoba, T., Tokutome, M., Funamoto, D., Katsuki, S., Ikeda, G., … Egashira, K. (2016). Nanoparticle-mediated delivery of irbesartan induces cardioprotection from myocardial ischemia-reperfusion injury by antagonizing monocyte-mediated inflammation. *Scientific Reports*, *6*, 29601. https://doi.org/10.1038/srep29601

Ntountaniotis, D., Andreadelis, I., Kellici, T. F., Karageorgos, V., Leonis, G., Christodoulou, E., … Mavromoustakos, T. (2019). Host-guest interactions between candesartan and its prodrug candesartan cilexetil in complex with 2-Hydroxypropyl-β-cyclodextrin: On the biological potency for angiotensin II antagonism. *Molecular Pharmaceutics*, *16*(3), 1255–1271. https://doi.org/10.1021/acs.molpharmaceut.8b01212

Oana, M., Tintaru, A., Gavriliu, D., Maior, O., & Hillebrand, M. (2002). Spectral study and molecular modeling of the inclusion complexes of β-Cyclodextrin with some phenoxathiin derivatives. *The Journal of Physical Chemistry B*, *106*(2), 257–263. https://doi.org/10.1021/jp012198v

Raja, B., Himasri, P., & Ramadevi, B. (2012). RP-HPLC Method for the simultaneous estimation of irbesartan and hydrochlorthiazide in pharmaceutical dosage form. *International Research Journal of Pharmaceutical and Applied Sciences*, *2*(3), 29–38.

Roe, D. R., & Cheatham, T. E. (2013). PTRAJ and CPPTRAJ: Software for processing and analysis of molecular dynamics trajectory data. *Journal of Chemical Theory and Computation*, *9*(7), 3084–3095. https://doi.org/10.1021/ct400341p

Ryckaert, J.-P., Ciccotti, G., & Berendsen, H. J. C. (1977). Numerical integration of the cartesian equations of motion of a system with constraints: Molecular dynamics of n-alkanes. *Journal of Computational Physics*, *23*(3), 327–341. https://doi.org/10.1016/0021-9991(77)90098-5

Salomon-Ferrer, R., Gotz, A. W., Poole, D., Le Grand, S., & Walker, R. C. (2013). Routine microsecond molecular dynamics simulations with AMBER on GPUs. 2. Explicit solvent particle mesh ewald. *Journal of Chemical Theory and Computation*, *9*(9), 3878–3888. https://doi.org/10.1021/ct400314y

Shahin, N. N., Abdelkader, N. F., & Safar, M. M. (2018). A novel role of irbesartan in gastroprotection against indomethacin-induced gastric injury in rats: Targeting DDAH/ADMA and EGFR/ERK signaling. *Scientific Reports*, *8*(1), 4280. https://doi.org/10.1038/s41598-018-22727-6

Soares da Silva, L. F., do Carmo, F. A., de Almeida Borges, V. R., Monteiro, L. M., Rodrigues, C. R., Cabral, L. M., & Desousa, V. P. (2011). Preparation and evaluation of lidocaine hydrochloride in cyclodextrin inclusion complexes for development of stable gel in association with chlorhexidine gluconate for urogenital use. *International Journal of Nanomedicine*, *6*, 1143–1154. https://doi.org/10.2147/ijn.s20409

Soma, D., Attari, Z., Reddy, M. S., Damodaram, A., & Koteshwara, K. B. G. (2017). Solid lipid nanoparticles of irbesartan: preparation, characterization, optimization and pharmacokinetic studies. *Brazilian Journal of Pharmaceutical Sciences*, *53*, 1–10.

Tamargo, J., Duarte, J., & Ruilope, L. M. (2015). New antihypertensive drugs under development. *Current Medicinal Chemistry*, *22*(3), 305–342.

Wang, J., Wolf, R. M., Caldwell, J. W., Kollman, P. A., & Case, D. A. (2004a). Development and testing of a general amber force field. *Journal of Computational Chemistry*, *25*(9), 1157–1174. https://doi.org/10.1002/jcc.20035

Wang, J., Wolf, R. M., Caldwell, J. W., Kollman, P. A., & Case, D. A. (2004b). Development and testing of a general amber force field. *Journal of Computational Chemistry*, *25*, 1157–1174. https://doi.org/10.1002/jcc.20035

Wang, W., & Kollman, P. A. (2001). Computational study of protein specificity: The molecular basis of HIV-1 protease drug resistance. *Proceedings of the National Academy of Sciences United States of*

America, *98*(26), 14937–14942. https://doi.org/10.1073/pnas.25126 5598

Wang, X., & Li, G. (2018). Irbesartan prevents sodium channel remodeling in a canine model of atrial fibrillation. *Journal of the Renin-Angiotensin-Aldosterone System*, *19*(1), 1470320318755269. https://doi.org/10.1177/1470320318755269

Yousef, F. (2018). Effect of pH on the complexation of irbesartan with β-, hydroxypropyl-β-, and γ-cyclodextrin: Solubility enhancement and physicochemical characterization. *Turkish Journal of Chemistry*, *42*(6), 1544–1558.

Yousif, N. G., Hadi, N. R., Al-Amran, F., & Zigam, Q. A. (2018). Cardioprotective effects of irbesartan in polymicrobial sepsis: The role of the p38MAPK/NF-kappaB signaling pathway. *Herz*, *43*(2), 140–145. https://doi.org/10.1007/s00059-017-4537-6

Zhang, F., Zhou, G., Guo, L., Lu, F., & Zhou, G. (2018). Comparison of clinical efficacy of metoprolol combined with irbesartan and hydrochlorothiazide and non-invasive ventilator in the emergency treatment of patients with severe heart failure. *Experimental and Therapeutic Medicine*, *16*(6), 5059–5066. https://doi.org/10.3892/etm.2018.6828

SUPPORTING INFORMATION

Additional supporting information may be found online in the Supporting Information section.